

# Disappearance of a Stacking Fault in Hard-Sphere Crystals under Gravity

Atsushu MORI,<sup>\*)</sup> Yoshihisa SUZUKI, and Shigeki MATSUO

*Institute of Technology and Science, The University of Tokushima, Tokushima  
770-8506, Japan*

In the first part of this paper, a review is given on the mechanism for the disappearance of an intrinsic stacking fault in a hard-sphere (HS) crystal under gravity, which we recently discovered by Monte Carlo (MC) simulations [A. Mori *et al.*, J. Chem. Phys. **124** (2006), 17450; Mol. Phys. **105** (2007), 1377]. We have observed, in the case of fcc (001) stacking, that the intrinsic stacking fault running along an oblique direction shrunk through the gliding of a Shockley partial dislocation at the lower end of the stacking fault. In order to address the shortcomings and approximations of previous simulations, such as the use of periodic boundary condition (PBC) and the fact that the fcc (001) stacking had been realized by the stress from the small PBC box, we present an elastic strain energy calculation for an infinite system and a MC simulation result for HSs in a pyramidal pit under gravity. In particular, the geometry of the latter has already been tested experimentally [S. Matsuo *et al.*, Appl. Phys. Lett. **82** (2003), 4283]. The advantage of using a pyramidal pit as a template as well as the feasibility of the mechanism we describe is demonstrated.

## §1. Introduction

In 1957, the existence of the crystalline phase in a hard-sphere (HS) system was found by Monte Carlo (MC) and molecular dynamics (MD) simulations;<sup>1),2)</sup> the crystalline phase transition in the HS system is sometimes referred to as the Alder transition. It was surprising that a system comprised merely of hard-core repulsion exhibited a phase transition. An intuitive understanding of the Alder transition is given by decomposing of the entropy into a contribution due to the configurational variation of the HSs' centers and a contribution due to the vibrational degree of freedom around the HSs' equilibrium positions. While the configurational entropy dominates in a disordered fluid phase, the vibrational entropy dominates in the crystalline phase. In the HS system the phase behavior is governed by the density; the system is in the fluid phase at a density lower than  $\phi_f$  and in the crystalline phase of a face-centered cubic (fcc) structure at a density higher than  $\phi_s$ . Here, the particle density is expressed in terms of the volume fraction of the HSs  $\phi \equiv \pi\sigma^3 N/6V$ , where  $\sigma$  is the HS diameter,  $N$  is the number of particles, and  $V$  is the total system volume. A crystal of  $\phi_s$  can coexist with a fluid of  $\phi_f$  when the volume fraction of the total system lies between  $\phi_f$  and  $\phi_s$ . The Hoover and Ree<sup>3)</sup> determined  $\phi_f = 0.494$  and  $\phi_s = 0.545$  by a MC method in 1968. Those values have been revised in the last decade to  $\phi_f = 0.491$  and  $\phi_s = 0.542$  by a MD simulation study of the direct two-phase coexistence (i.e., the crystal/fluid interface).<sup>4)</sup> We note that even the first MD simulation of the HS crystal/fluid interface was successfully performed within the last decade.<sup>5)</sup>

---

<sup>\*)</sup> E-mail: mori@opt.tokushima-u.ac.jp

The present situation is a little different from that in the early years. In the 1960s and -70's, the existence of colloidal crystals drew much interest as an experimental realization of the Alder transition. The effective HS picture was proposed for charged colloids, which interacts through a screened Coulomb potential where the interparticle interaction is thus well described by a repulsive Yukawa form.<sup>6)</sup> Today, the HS system is not just an effective model of the colloids; poly(methylmethacrylate) (PMMA) particles with stabilizing polymers grafted on the particle's surface<sup>7)</sup> were developed as HS suspensions. The PMMA particles were dispersed in a compounded hydrocarbon medium so that the HS nature with regards to the crystal-melt phase transition was exhibited.<sup>7),8),9),10),11)</sup>

It should also be noted that colloidal crystals can possibly be used as materials for photonic crystals.<sup>12)</sup> To realize a photonic band, the defects in the colloidal crystal should be reduced. To this end, many techniques have been developed. One of them is colloidal epitaxy, in which a patterned substrate is used as a template to fix the stacking direction to be [001] in the sedimentation of the colloidal particles.<sup>13)</sup> Various patterns for the template have been examined, but in this work only a single pyramidal pit<sup>14)</sup> is considered.

In order to improve the quality of the colloidal crystal, the effect of gravity on the crystallinity of the colloidal crystal must be taken into account. Zhu *et al.*<sup>15)</sup> performed a colloidal crystallization on the Space Shuttle and concluded that under microgravity, a random hexagonal close pack (rhcp) was found. On the other hand, under normal gravity, the colloidal crystal formed by sedimentation is a rhcp/fcc mixture although the colloids sometimes freeze into a glassy state. Here, rhcp is the random stacking of hexagonal planes (fcc {111} or hcp (0001)); viewed along  $\langle 111 \rangle$ , the fcc is of ABCABC $\cdots$  type, and the hcp is of ABAB $\cdots$  type while the rhcp corresponds to a random sequence. In other words, the stacking disorder can be reduced by gravity. We have, however, not found a final answer to the stacking sequence of colloidal crystals under gravity. Although the gravitational constant  $g^* \equiv mg\sigma/k_B T$  was different, Kegel and Dhont<sup>16)</sup> observed a faulted twinned fcc under gravity. Here,  $m$  is the particle's mass,  $g$  is the acceleration due to gravity,  $\sigma$  is the HS diameter, and  $k_B T$  is the temperature multiplied by Boltzmann's constant. We note that the temperature  $T$  should be defined from the thermal motion of the dispersing particles.

This paper focuses on the mechanism of the disappearance of the stacking disorder in a HS crystal under gravity. We have already demonstrated the disappearance of stacking disorder in a HS crystal under gravity by MC simulations.<sup>17)</sup> We have examined closely where the shrinking of an intrinsic stacking fault was observed.<sup>18)</sup> In § 2, we review those simulation results, point out their shortcomings, and reiterate the mechanism of the defect disappearance that had been found. The objective of this paper is to provide new results to complement these shortcomings. The systems<sup>17),18)</sup> were highly stressed because of their smallness. We present some results of the elastic energy calculation for an infinite system in § 3. The periodic boundary condition (PBC) applied in the previous simulations<sup>17),18)</sup> was one of the artifacts that needed to be addressed. In § 4 we present results of the MC simulation for realizable boundary conditions by simulating HSs in a pyramidal pit.<sup>14)</sup>

## §2. Monte carlo simulation under the PBC

In previous simulations,<sup>17)</sup> we presented results for two system sizes. One contained  $N=1664$  particles and the other  $N=3744$ . In the former, fcc (001) stacking occurred, while in the latter, stacking of the hexagonal layers took place. We concentrated on the former<sup>18)</sup> because the defects' disappearance was observed in this case. Although the side length equaled  $4a_0$ , six particles lay along a side. Here,  $a_0 = 1.57\sigma = (4\sigma^3/\rho_s)^{1/3}$  was the fcc lattice constant at the crystal/fluid coexistence of Hoover and Ree's value<sup>3)</sup> with  $\rho$  denoting the particle density [ $\phi \equiv (\pi/6)\rho\sigma^3$ ]. Six unit cells lay along the diagonal direction. In other words, the [010] and [100] are directed to the diagonal directions.<sup>19)</sup> This indicated that the crystal at the bottom was at a higher pressure than the crystal-fluid coexistence pressure [the Hoover and Ree's value is  $(P\sigma^3/k_B T)_{coex} = 11.75^3)$  and Davidchack and Laird's value 11.55<sup>4)</sup>] in accordance with the mechanical balance equation

$$\partial P/\partial z = -mg\rho(z) \quad (2.1)$$

at the sedimentation equilibrium, where  $\rho(z)$  is the particle density on a coarse-scale at altitude  $z$ . Also, (2.1) implies that the lattice spacing along  $z$  direction varies and that the unit cell is compressed along the vertical direction, i.e., the crystal is no longer a cubic system, as was previously confirmed.<sup>19)</sup> The disappearance of the stacking fault occurred under such artificially stressed condition. Such stress, however, plays a central role in defect reduction. As shall be described below, the (001) stacking, in which the shrinking of the stacking fault occurred,<sup>18)</sup> was thereby induced. Moreover, some researchers made an efforts to realize the (001) growth, such as the colloidal epitaxy,<sup>13)</sup> with the understanding that the stacking sequence for this growth is unique. Concentrating on phenomena occurring under the (001) stacking without particularly concerning ourselves with the experimental realization of this stacking is one of paths to elucidation of the defect reduction mechanism.

In previous simulations,<sup>17),18)</sup> the gravitational constant,  $g^*$ , was changed in a step-wise fashion in order to avoid trapping the system in a metastable state such as a polycrystalline state.<sup>20)</sup> We set  $g^*$  to a certain value for  $2 \times 10^5$  MC cycle (MCC),

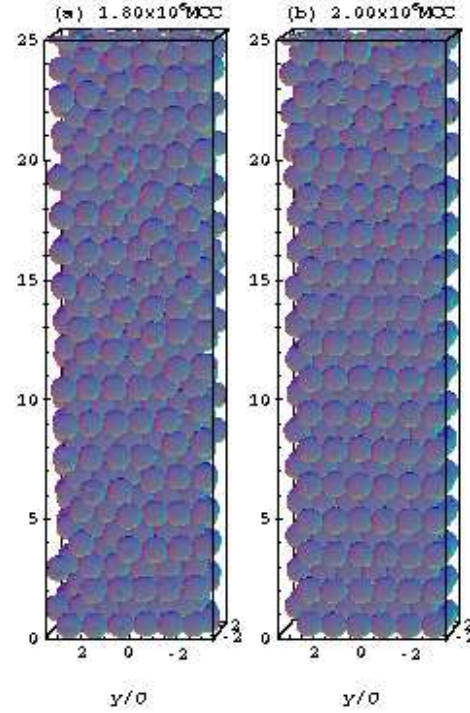


Fig. 1. Snapshots at (a) the beginning and (b) the end of a MC simulation<sup>17)</sup> with  $g^*$  fixed at 0.9.

and then changed  $g^*$  by an amount of  $\Delta g^* = 0.1$ , where one MCC is defined so as to include, on average, one position move per particle. Transformation of a defective crystal into a less-defective crystal was observed for the case of (001) stacking for  $g^*$  around  $g^* = 0.9$ .<sup>17)</sup> While  $g^*$  was kept at 0.9 for the (001) stacking case, we found that the shrinking of an intrinsic stacking fault was mediated by the glide of the Shockley partial dislocation terminating at the bottom end of the stacking fault running in the oblique direction.<sup>18)</sup> In Fig. 1 we see a disappearance of the stacking faults, which run from the lower-left to the middle-right, [see, Ref. 18) for details of the shrinking of the intrinsic stacking fault]. We stress that the advantage of the (001) stacking is not only the uniqueness of the stacking sequence but also the glide mechanism of the Shockley partial dislocation.

### §3. Elastic strain energy consideration

In this section, we present the elastic energy calculation for a system including an intrinsic stacking fault running along the [111]. The lower end of the stacking fault is terminated by a Shockley partial dislocation, such as the one shown in Ref. 18) and illustrated in Fig. 2. In this paper, we incorporated the effect of gravity as buoyancy due to the particle deficiency accompanied by the dislocation core. The particle deficiency is one-third in Fig. 2. Though the crystal was indeed strained due to gravity,<sup>19)</sup> which coupled with the stress due to the Shockley partial dislocation to help promote the shrinking of the intrinsic stacking fault, we can understand the shrinking of the intrinsic stacking fault without considering the cross coupling between these stresses.

The Shockley partial dislocation terminating an intrinsic stacking fault running along the [111] (as shown in Fig. 2) is defined by the Burgers vector  $\mathbf{b}^I = (1/6)[\bar{2}11] \equiv -\mathbf{a}_1/3 + \mathbf{a}_2/6 + \mathbf{a}_3/6$  with  $\mathbf{a}_1$ ,  $\mathbf{a}_2$ , and  $\mathbf{a}_3$  being the lattice vectors, which is shown by the arrow in Fig. 3. We can understand the partial dislocation by the decomposition of a perfect dislocation. In Fig. 3, the Burgers vector of a perfect dislocation,  $\mathbf{b} = (1/2)[\bar{1}10]$ , is decomposed as  $\mathbf{b} =$

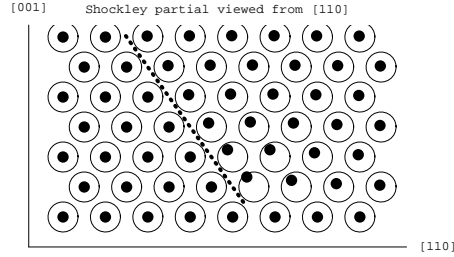


Fig. 2. Illustration of an intrinsic stacking fault. Particles in the distorted crystal are indicated by dots, and the regular lattice positions are indicated by open circles. The dotted line indicates the stacking fault. For simplicity, particles outside the portion right of stacking fault are not displaced in this illustration.

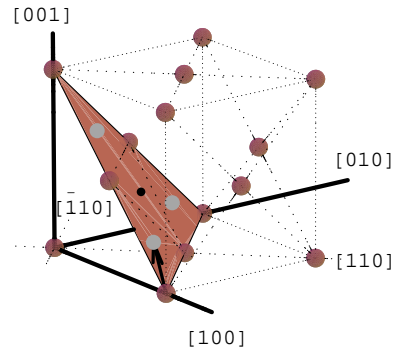


Fig. 3. The Burgers vector  $\mathbf{b}^I = (1/6)[\bar{2}11]$  (arrow) and the (111) plane (painted). The arrow connects a lattice position to an adjacent lattice position, say lattice point A to lattice point B.

$\mathbf{b}^I + \mathbf{b}^{II}$  with  $\mathbf{b}^{II} = (1/6)[\bar{1}2\bar{1}]$  as was done in Ref. 21).

We calculated the elastic energy due to a dislocation running along a unit vector  $\boldsymbol{\xi}$  using the following formula from isotropic, linear elastic theory<sup>21)</sup>

$$W(R) = \frac{\mu b^2}{4\pi} \left( \cos^2 \theta + \frac{\sin^2 \theta}{1 - \nu} \right) \ln \left( \frac{\alpha R}{b} \right), \quad (3.1)$$

where  $\mu$ ,  $\nu$ , and  $\theta$  are the shear modulus, the Poisson ratio, and the angle between the Burgers vector  $\mathbf{b}$  and  $\boldsymbol{\xi}$ , respectively, and  $b$  denotes  $|\mathbf{b}|$ . Here, with  $\alpha$ , which is several tenths, the radius of defined core region is  $r_0 \equiv b/\alpha$ , and  $R$  is the dimension over which the elastic field expands, which we can usually identify with the crystallite or grain radius. In the present case, where the stacking fault is running upward along the  $\langle 111 \rangle$  starting at the position of the Shockley partial dislocation, we simply set  $R$  to the distance from the upper boundary to the Shockley partial dislocation. (Note that the dependence of the geometry of the boundary or the shape of the crystallite is ignored.) Substituting  $\mathbf{b}^I$  for  $\mathbf{b}$  (i.e.,  $|\mathbf{b}^I| = a/\sqrt{6}$  with  $a$  being the fcc lattice constant) and  $\boldsymbol{\xi} = (1/\sqrt{2})[\bar{1}10]$  (i.e.,  $\theta = \pi/6$ ), we obtain an elastic energy of

$$U_{el} = \frac{\mu a^2}{96\pi} \left( 3 + \frac{1}{1 - \nu} \right) \ln \left( \frac{\sqrt{6}\alpha R}{a} \right). \quad (3.2)$$

Hereafter, we consider a system of unit length thickness perpendicular to Fig. 2. The core region is defined so that linear elastic theory is still valid outside that region. Borrowing the empirical result for metals,<sup>21)</sup> the core energy  $U_{core}$  is proportional to  $\mu b^2$ . Let us write  $U_{core} = \beta \mu b^2$  with  $\beta$  being a certain constant of order less than unity. We have

$$U_{core} = \beta \mu a^2 / 6, \quad (3.3)$$

( $\mathbf{b} = \mathbf{b}^I$ ) for the intrinsic stacking fault. Note that (3.3) is independent of  $R$ .

We should now consider the stacking fault energy. This quantity, as well as the elastic and core energies (rigorously, the free energies), is an entropic contribution resulting from the variation of the vibrational mode distribution. Though the core energy has not been calculated, the shear modulus  $\mu$  was calculated by a MC simulation<sup>22)</sup> and density functional theory,<sup>23)</sup> and the stacking fault energy  $\gamma_{sf}$  was calculated by a MC simulation.<sup>24)</sup> The quantity,  $\mu\sigma^3/k_B T$  for the HS crystal ranges between 50 and 100, depending on the particle number density,  $\rho$ . This range of  $\mu$  corresponds to  $\rho\sigma^3 \cong 1.06 - 1.13$  ( $a/\sigma \cong 1.55 - 1.52$ ) where the disappearance of the stacking disorder was observed in the MC simulations.<sup>17),18)</sup> The stacking fault interfacial energy per unit area,  $\gamma_{sf}\sigma^2/k_B T$ , was (at most) of the order  $10^{-4}$  at  $\rho\sigma^3 = 1.10$ . The difference of the orders in  $\mu$  and  $\gamma_{sf}$  has a crucially important meaning; if the perfect dislocation is decomposed into two partial dislocations connected by a stacking fault, the separation between two partial dislocations would be much longer than the order of the crystallite radius, which is typically a few to several hundred lattice spacings. The total stacking fault energy is obtained by multiplying the length of the stacking fault, which is  $\zeta R$ ; the proportional constant  $\zeta$  depends on the geometry of the boundary. Thus, we have  $U_{sf} = \zeta \gamma_{sf} R$ .

The gravitational energy is solely given by  $U_g(R) - U_g(0) = m\rho a^2 R/3$ , where we have neglected the dependence of the particle density on the altitude. This approximate treatment was consistent with the treatment where we neglected the deformation according to (2.1). Here  $U_g(R)$  is the gravitational energy where the lower end of the stacking fault is located from the upper boundary of the crystallite; so  $U_g(0)$  vanished because the stacking fault went out of the crystallite when  $R = 0$ . The sum of gravitational energy and the stacking fault energy was thus a linear function

$$U_{sf} + U_g = (\zeta\gamma_{sf} + m\rho a^2/3)R. \quad (3.4)$$

The total energy,  $U_{el} + U_{core} + U_{sf} + U_g$ , is comprised of a logarithmic term (3.2), a constant (3.3), and a linear term (3.4). The coefficient of the logarithmic term is positive and that of the linear term is also apparently positive. This means that as  $R$  decreases, the energy decreases. We have shown by an elastic calculation that in the (001) stacking, gravity provided a driving force that promoted the glide of the Shockley partial dislocation upwards.

#### §4. Monte carlo simulation of hard spheres in a pyramidal pit

In the preceding two sections, we considered two systems with artificial boundary conditions. In contrast, in this section, we treat a realistic boundary condition. Matsuo *et al.*<sup>14)</sup> used a pyramidal pit and groove to fix the stacking sequence. A pyramidal pit can be made by the anisotropic etching of the Si (001) surface (Fig. 4).

Contrary to the simulations with PBC, the crystallinity was less sensitive to how  $g^*$  was controlled. This may be due to wetting on the edges of the pyramidal pit (Fig. 5(a)). In Fig. 5, snapshots of MC simulations at  $g^* = 0.1$  and 1.5 are shown; though  $\Delta t = 2$  and  $4 \times 10^5 \text{MCC}$ , where  $g^*$  was kept constant, were also tested, only the results for  $\Delta t = 1 \times 10^5 \text{MCC}$  are shown. Figure 5(b) shows that despite the edge wetting, the particles at the bottom were not crystallized. On the other hand, the particles were crystallized at the bottom of the pit, particularly, in the fcc (001) stacking. In the pyramidal pit made of the  $\{111\}$  faces, which can be experimentally generated, the (001) stacking has been confirmed, as was already experimentally demonstrated.<sup>14)</sup> Unfortunately, looking over the snapshots, we could not find the stacking faults, and thus, the glide mechanism of the stacking fault disappearance was not observed. In our opinion, however, this was an indication of this method's robustness against stacking disorder; the epitaxial growth at the late stage started from the edges of the pit where the wetting occurred. In addition,

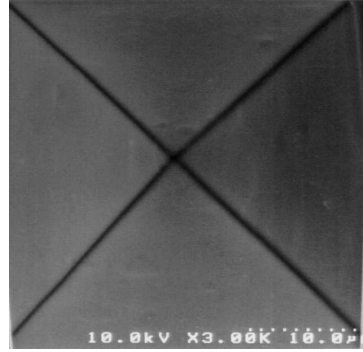


Fig. 4. A top view of a pyramidal pit made of four Si  $\{111\}$  faces (scanning microscopy image).

the geometry of the boundary was advantageous; even if a crystallite mismatched its crystallographic orientation or lateral position with the formed crystal as it nucleates at the bottom, the crystallite could slide along the wall. In other words, the simulation results did not rule out the glide mechanism of a stacking fault but instead emphasised its role.

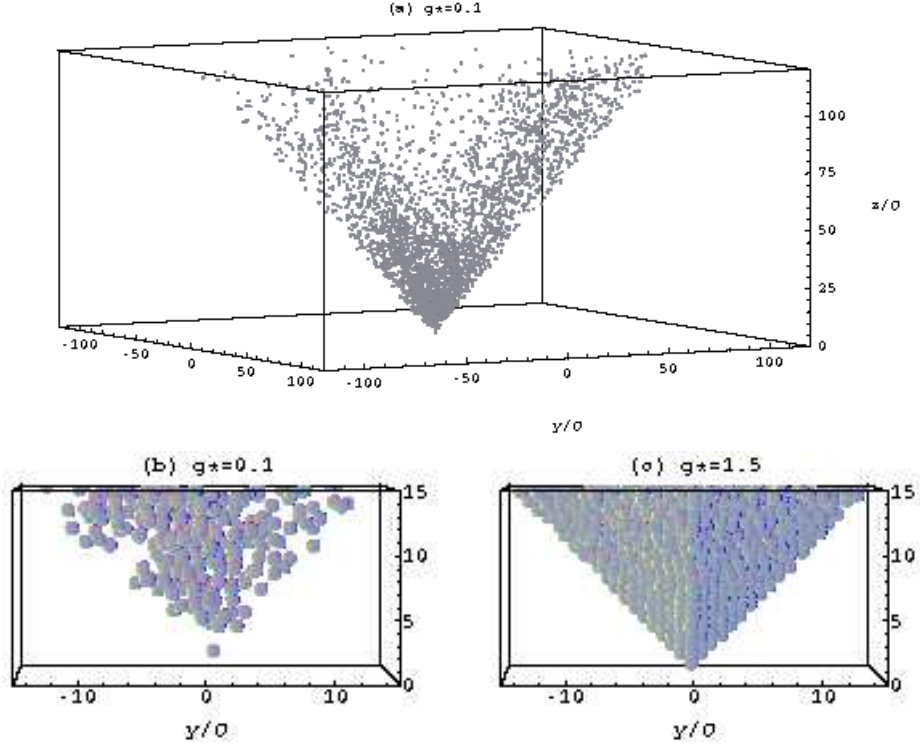


Fig. 5. Snapshots of MC simulation of the HSs in a pyramidal pit. (a) An overview at  $g^*=0.1$ , where edge wetting is seen, (b) a magnification of (a), and (c) a magnified snapshot at  $g^*=1.5$ , where crystalline order was observed.

## §5. Discussions

Here we compare two simulations. Under PBC, the configuration is equivalent to the dislocation array of the same Burgers vector. On the other hand, owing to the concept of the mirror image, the pyramidal pit system is equivalent to an array of opposite charges. Whereas the former is less mobile, the dislocation in the latter more easily disappears, which can be understood by pair annihilation of opposite charges. The glide mechanism is likely implicated because it was observed in the former configuration.

The cross term between the gravity-induced elastic field and the stress due to dislocation has not been treated in this paper. From (2.1), the particle density decreases as the altitude increases. This means that the buoyancy of the dislocation

core is promoted as the core goes up because the higher the altitude is, the looser the packing is. Essentially the same argument can be valid for the strain energy to due the dislocation.

## §6. Concluding remarks

We presented two simulation results and one theoretical calculation. All of our results support the glide mechanism for the disappearance of the stacking disorder in a hard-sphere crystal under gravity. We wish to emphasize that although this mechanism is not the final unique answer, it is likely to occur.

In a theoretical elastic calculation, we can understand the glide mechanism without taking into account the cross term between the gravity-induced elastic field and the stress due to the dislocation. That is,  $\partial\sigma_{ij}/\partial x_i = 0$  has been solved, where  $\sigma_{ij}$  is the stress tensor. The rigorous treatment is to solve  $\partial\sigma_{ij}/\partial x_i + f_i = 0$  with  $f_i$  denoting the external force (gravitational force in the present case). This calculation is currently underway using the results from Ref. 19).

## References

- 1) W. W. Wood and J. D. Jacobson, J. Chem. Phys. **27** (1957), 1207.
- 2) B. J. Alder and T. E. Wainwright, J. Chem. Phys. **27** (1957), 1208.
- 3) W. G. Hoover and F. H. Ree, J. Chem. Phys. **49** (1968), 3609.
- 4) R. L. Davidchack and B. B. Laird, J. Chem. Phys. **108** (1998), 9452.
- 5) A. Mori, R. Manabe and K. Nishioka, Phys. Rev. E **51** (1995), R3831.
- 6) M. Wadati and M. Toda, J. Phys. Soc. Jpn. **32** (1972), 1147.
- 7) L. Antl, J. W. Goodwin, R. D. Hill, R. H. Ottewil, S. M. Owens, S. Parworth and J. W. Waters, Colloids Surf. **17** (1986), 67.
- 8) P. N. Pusey and W. van Megen, Nature **320** (1986), 340.
- 9) S. E. Paulin and B. J. Ackerson, Phys. Rev. Lett. **64** (1990), 2663.
- 10) S. M. Underwood, J. R. Taylor and W. van Megen, Langmuir **10** (1994), 3550.
- 11) S. E. Phan, W. B. Russel, Z. Cheng, J. Zhu, P. M. Chaikin, J. H. Dunsмур and R. H. Ottewil, Phys. Rev. E **54** (1996), 6633.
- 12) K. Sakoda, *Optical Properties of Photonic Crystal* (Springer-Verlag, Bargin, 2001).
- 13) A. van Blaaderen, R. Ruel and P. Wiltzius, Nature **385** (1997), 321.
- 14) S. Matsuo, T. Fujine, K. Fukuda, S. Joudokazis and H. Misawa, Appl. Phys. Lett. **82** (2003), 4283.
- 15) J. Zhu, M. Li, R. Rogers, W. Mayer, R. H. Ottewil, STS-73 Space Shuttle Crew, W. B. Russel and P. M. Chaikin, Nature **387** (1997), 883.
- 16) W. K. Kegel and J. K. G. Dhont, J. Chem. Phys. **112** (2000), 3431.
- 17) A. Mori, S.-i. Yanagiya, Y. Suzuki, T. Sawada and K. Ito, J. Chem. Phys. **124** (2006), 174507.
- 18) A. Mori, Y. Suzuki, S.-i. Yanagiya, T. Sawada and K. Ito, Mol. Phys. **105** (2007), 1377.
- 19) A. Mori, S.-i. Yanagiya, Y. Suzuki, T. Sawada and K. Ito, Sci. Technol. Adv. Mater. **7** (2006), 296.
- 20) S.-i. Yanagiya, A. Mori, Y. Suzuki, Y. Miyoshi, M. Kasuga, T. Sawada, K. Ito and T. Inoue, Jpn. J. Appl. Phys. (Part 1) **44** (2005), 5113.
- 21) J. P. Hirth and J. Lothe, *Theory of dislocations* (Krieger, Melabar, 1982).
- 22) D. Frenkel and A. J. C. Ladd, Phys. Rev. Lett. **59** (1987), 1169.
- 23) B. B. Laird, J. Chem. Phys. **97** (1992), 2699.
- 24) S. Pronk and D. Frenkel, J. Chem. Phys. **110** (1999), 4589.



**Errata [Prog. Theor. Phys. Suppl. 178 (2009), 33.]**

Both in Eq. (3.2) and on the line 5 on page 38 (6th page), we should add a prefactor  $(1/2\sqrt{2})$  on  $m\rho a^2/3$  and  $m\rho a^2 R/3$ , respectively. This factor arises from the area per  $[\bar{1}10]$  line on  $(110)$  plane, which is  $a^2/2\sqrt{2}$ . We can also derive this by considering the number of particles on  $[\bar{1}10]$  per unit length, i.e.,  $U_g = m(\sqrt{2}/a)/3 = (1/2\sqrt{2})m\rho a^2/3$  because  $\rho = 4/a^3$  for fcc lattice.